

## On Improving 4-km Mesoscale Model Simulations

AIJUN DENG AND DAVID R. STAUFFER

*Department of Meteorology, The Pennsylvania State University, University Park, Pennsylvania*

(Manuscript received 13 December 2004, in final form 11 August 2005)

### ABSTRACT

A previous study showed that use of analysis-nudging four-dimensional data assimilation (FDDA) and improved physics in the fifth-generation Pennsylvania State University–National Center for Atmospheric Research Mesoscale Model (MM5) produced the best overall performance on a 12-km-domain simulation, based on the 18–19 September 1983 Cross-Appalachian Tracer Experiment (CAPTEX) case. However, reducing the simulated grid length to 4 km had detrimental effects. The primary cause was likely the explicit representation of convection accompanying a cold-frontal system. Because no convective parameterization scheme (CPS) was used, the convective updrafts were forced on coarser-than-realistic scales, and the rainfall and the atmospheric response to the convection were too strong. The evaporative cooling and downdrafts were too vigorous, causing widespread disruption of the low-level winds and spurious advection of the simulated tracer. In this study, a series of experiments was designed to address this general problem involving 4-km model precipitation and gridpoint storms and associated model sensitivities to the use of FDDA, planetary boundary layer (PBL) turbulence physics, grid-explicit microphysics, a CPS, and enhanced horizontal diffusion. Some of the conclusions include the following: 1) Enhanced parameterized vertical mixing in the turbulent kinetic energy (TKE) turbulence scheme has shown marked improvements in the simulated fields. 2) Use of a CPS on the 4-km grid improved the precipitation and low-level wind results. 3) Use of the Hong and Pan Medium-Range Forecast PBL scheme showed larger model errors within the PBL and a clear tendency to predict much deeper PBL heights than the TKE scheme. 4) Combining observation-nudging FDDA with a CPS produced the best overall simulations. 5) Finer horizontal resolution does not always produce better simulations, especially in convectively unstable environments, and a new CPS suitable for 4-km resolution is needed. 6) Although use of current CPSs may violate their underlying assumptions related to the size of the convective element relative to the grid size, the gridpoint storm problem was greatly reduced by applying a CPS to the 4-km grid.

### 1. Introduction

An interregional transport study was conducted by Deng et al. (2004) using the fifth-generation Pennsylvania State University (PSU)–National Center for Atmospheric Research Mesoscale Model (MM5). It was found that a baseline model configuration reflecting typical capabilities of the late 1980s [70-km horizontal grid, 15 vertical layers, older subgrid physics, and no four-dimensional data assimilation (FDDA)] produced large meteorological errors that severely degraded the accuracy of the surface (perfluorocarbon) tracer concentrations predicted by the Second-Order Closure In-

tegrated Puff (SCIPUFF) transport and dispersion model (Sykes et al. 1996). Improving the horizontal and vertical resolution of MM5 to 12 km (typical for current operational models) and 32 layers led to some improvements in the statistical skill, but the further addition of more advanced physics produced greater reductions of simulation errors. Use of FDDA, along with 12-km resolution and improved physics, produced the overall best performance.

However, further reduction of the grid length from 12 to 4 km in the simulation of the 18–19 September 1983 Cross-Appalachian Tracer Experiment (CAPTEX) case had detrimental effects on the meteorological and plume dispersion solutions. The primary cause of the poor mesoscale model performance was likely the explicit (grid resolved) representation of convection accompanying a cold front advancing across the lower Great Lakes and into New England. Because no con-

Corresponding author address: Aijun Deng, Department of Meteorology, The Pennsylvania State University, University Park, PA 16802.  
E-mail: deng@essc.psu.edu

vective parameterization scheme (CPS) was used on the 4-km grid, the convective updrafts were forced on coarser-than-realistic scales (normal updraft diameter for most storms in the eastern United States is  $\sim 2$  km), and the rainfall and the atmospheric response to the convection were too strong. The evaporative cooling and the associated downdrafts from these gridpoint storms were too vigorous, causing widespread disruption of the low-level winds and spurious advection of the simulated tracer. This result should not be interpreted to mean that 4-km grids are unsuitable for air-quality studies in general; however, model simulations on a grid of 4 km or less cannot be automatically assumed to be superior to coarser-resolution simulations in all situations.

Figure 1 shows that fully explicit approaches cannot provide a general solution for models with grid resolution exceeding  $\sim 4$  km because convective updrafts are generally smaller than 4 km and the atmospheric convection has to be parameterized (Deng et al. 2003; Tao et al. 2003). Although CPSs have been successful at grid scales exceeding  $\sim 10$  km, they fail on the smaller scales because the scale-separation assumption is no longer valid (e.g., Molinari and Dudek 1992). In a study on the resolution dependence of explicitly modeled convective systems, Weisman et al. (1997) has shown that, although degradation was found in the model response as the resolution is decreased, resolution of 4 km was sufficient to reproduce much of the mesoscale structure and evolution of a squall-line-type convective system. Bryan et al. (2003), however, suggest that much finer model resolutions of order 100 m are needed to represent accurately the details of squall-line convection. Thus, accurate representation of modeled convection on the 1–5-km scales requires proper attention to the details of the microphysics and subgrid turbulence parameterization in both the vertical and horizontal dimensions. However, there are also issues with the turbulence parameterizations when the horizontal grid length is comparable to the depth of the mixed layer (Fig. 1).

Because there are no CPSs suitable for the 4-km scale at present, various MM5 sensitivity experiments are designed to find a best approach to improve the 4-km model simulations. Possible approaches include use of data assimilation (important for retrospective air-quality studies), use of improved PBL physics, microphysics, use of an existing CPS on the 4-km grid, and numerical diffusion. Thus, the objectives of this paper are to investigate the role of 1) data assimilation, 2) model physics, and 3) numerical diffusion on the accuracy of cloud and precipitation fields and associated flow fields simulated at  $\Delta x = 4$  km during CAPTEX-83.

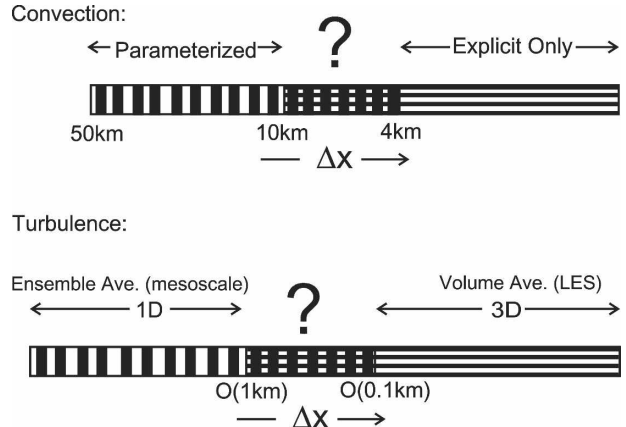


FIG. 1. A schematic illustrating the horizontal grid-scale ( $\Delta x$ ) dependence of convection and turbulence parameterizations. The crosshatched regions indicate where the underlying assumptions of the physical parameterizations are not strictly valid, and there is currently no robust, satisfactory solution in these “no-man’s land” scale ranges: convection ( $\sim 4$ –10 km  $\Delta x$ ) and turbulence ( $\Delta x \sim$  depth of mixed layer). Note that mesoscale turbulence schemes account only for vertical mixing and use ensemble-average assumptions for its flux calculations, whereas large-eddy simulations employ volume-average flux formulations.

A brief description of the CAPTEX-83 case is given in section 2. Section 3 of this paper describes the numerical model, physics options, and FDDA techniques applied to this study. The experimental design is given in section 4, and the model results are presented in section 5. A summary of the most relevant findings is given in section 6.

## 2. Overview of the 18–19 September CAPTEX-83 case

The case chosen in this study is the 18–19 September episode from CAPTEX-83, the same case that was used in the previous study (Deng et al. 2004). The meteorological conditions of this case were characterized by a large anticyclone centered over the Mid-Atlantic coast, with broad southwesterly wind flow over the midwestern and northeastern United States. To the northwest of the high pressure area, a frontal system was propagating rapidly through the western Great Lakes. Associated with the propagating frontal system, a low-level jet was a dominant feature at night, and it played a significant role in transporting the tracer material.

Surface observations over the midwestern and northeastern United States indicate that at 1200 UTC 18 September 1983 there are many thunderstorms close to the warm front from southeastern Wisconsin to southern Michigan, with widespread showers throughout the rest of Michigan. The rain then shifts eastward with the advancing warm front, so that by 1800 UTC the rain

showers are mostly around Lake Ontario before weakening at 0000 UTC 19 September. Later during the night, by 0600 UTC, thunderstorm activity and showers again become more widespread along the cold-frontal boundary and ahead of the warm front. These reinvigorated storms persisted through the night, mostly along the cold front, but weakened toward morning, especially from Lake Erie to Montreal, Quebec, Canada. Satellite imagery at 0830 UTC (not shown) and surface observations at 0900 UTC 19 September (Fig. 2a) confirm that convective clouds existed over the Great Lakes area, although there was no precipitation reported. By 1800 UTC 19 September (Fig. 2b), no frontal showers were observed in the Northeast, although cloudy skies are found farther to the north of the cold front. The 24-h total precipitation distribution over the eastern United States on 19 September 1983 (not shown) indicates that insignificant amounts of precipitation ( $<0.5$  mm) were observed over the Lake Erie region and somewhat larger amounts ( $<10$  mm) were observed southeast of Lake Ontario. At both 0900 and 1800 UTC the observed surface winds show southwesterly flow through most of Ohio and Pennsylvania ( $<10$  m s $^{-1}$ ).

### 3. Model description

The meteorological model used in this study is the nonhydrostatic MM5 (Dudhia 1993; Grell et al. 1994). As in the original study by Deng et al. (2004), grid sizes of 108, 36, 12, and 4 km are used with one-way nesting. On all of these domains, resolved-scale moist processes are represented using explicit prognostic equations for cloud water or ice and rainwater or snow according to a formulation described by Dudhia (1989). One experiment also includes mixed-phase processes (Reisner et al. 1998).

Two different CPSs are used: the Kain–Fritsch scheme (Kain and Fritsch 1990, 1993; Kain 2004) (KF) and the Grell scheme (Grell 1993; Grell et al. 1994). The Grell CPS is a mass-flux-based scheme that contains an entraining/detraining cloud model that involves both updraft and downdraft. Its closure depends on quasi equilibrium between the large-scale rate of convective destabilization and localized rate of stabilization by (parameterized) convection. The Kain–Fritsch scheme has a fully entraining/detraining cloud model and uses an energy-equilibrium closure based on convective available potential energy (CAPE) removal.

The ground temperature is predicted based on a surface energy budget (slab force–restore method) that includes the effects of atmospheric radiation and the surface fluxes, which vary based on specified land-use

information and soil moisture (Grell et al. 1994). The Rapid Radiative Transfer Model (RRTM; Mlawer et al. 1997) is used for longwave radiation, and the Dudhia scheme (Grell et al. 1994) is used for shortwave radiation. The Dudhia radiation scheme is based on a two-stream, single-band approach, which is fully interactive with dry air, water vapor, and cloud liquid/ice.

Two different types of planetary boundary layer (PBL) turbulence parameterizations are used in this study: a widely used first-order closure scheme known as the Hong and Pan Medium-Range Forecast (MRF) PBL (Hong and Pan 1996), and a 1.5-order closure turbulent kinetic energy (TKE) prediction scheme, the PSU Gayno–Seaman PBL (GS PBL; Shafran et al. 2000; Stauffer et al. 1999). The TKE-predicting GS PBL scheme is representative of newer higher-order PBL physics and has been shown to generate both shear-driven turbulence and realistic in-cloud mixing associated with cloud-top radiative flux divergence (Stauffer et al. 1999).

FDDA is commonly used for improved model initialization (dynamic initialization) or data analysis (dynamic analysis). FDDA, when used for dynamic analysis, is a process in which observations are used continuously throughout a model simulation to correct numerical forecast errors, instead of using data only at the initial time. It is widely used by the air-quality community and has been shown to reduce error significantly for air-quality studies in which the meteorological model fields are used to drive an air-chemistry model or transport and dispersion model (e.g., Tanrikulu et al. 2000; Seaman 2000; Deng et al. 2004).

The FDDA approach by Stauffer and Seaman (1990, 1994) and Stauffer et al. (1991) uses “nudging” to relax the model solutions toward the observations continuously at each time step by adding to the prognostic equations an artificial tendency term, which is based on the difference between the two states (i.e., the innovation), the nudging coefficient  $G$ , and spatial and temporal weighting functions. The assimilation can be accomplished by nudging the model solutions toward gridded analyses based on observations (analysis nudging, hereinafter Analysis FDDA) or directly toward the individual observations (observational nudging, herein-after Obs FDDA). In the work presented in this paper, both Analysis FDDA and Obs FDDA are used.

For asynoptic observations, sparse data, or meso-beta-scale model simulations, especially in complex terrain, a realistic analysis of observations cannot be easily performed and Obs FDDA is the preferred technique. Obs FDDA computes the innovation at each observation site and applies a weighted correction to a neighborhood of grid points that surround the observation

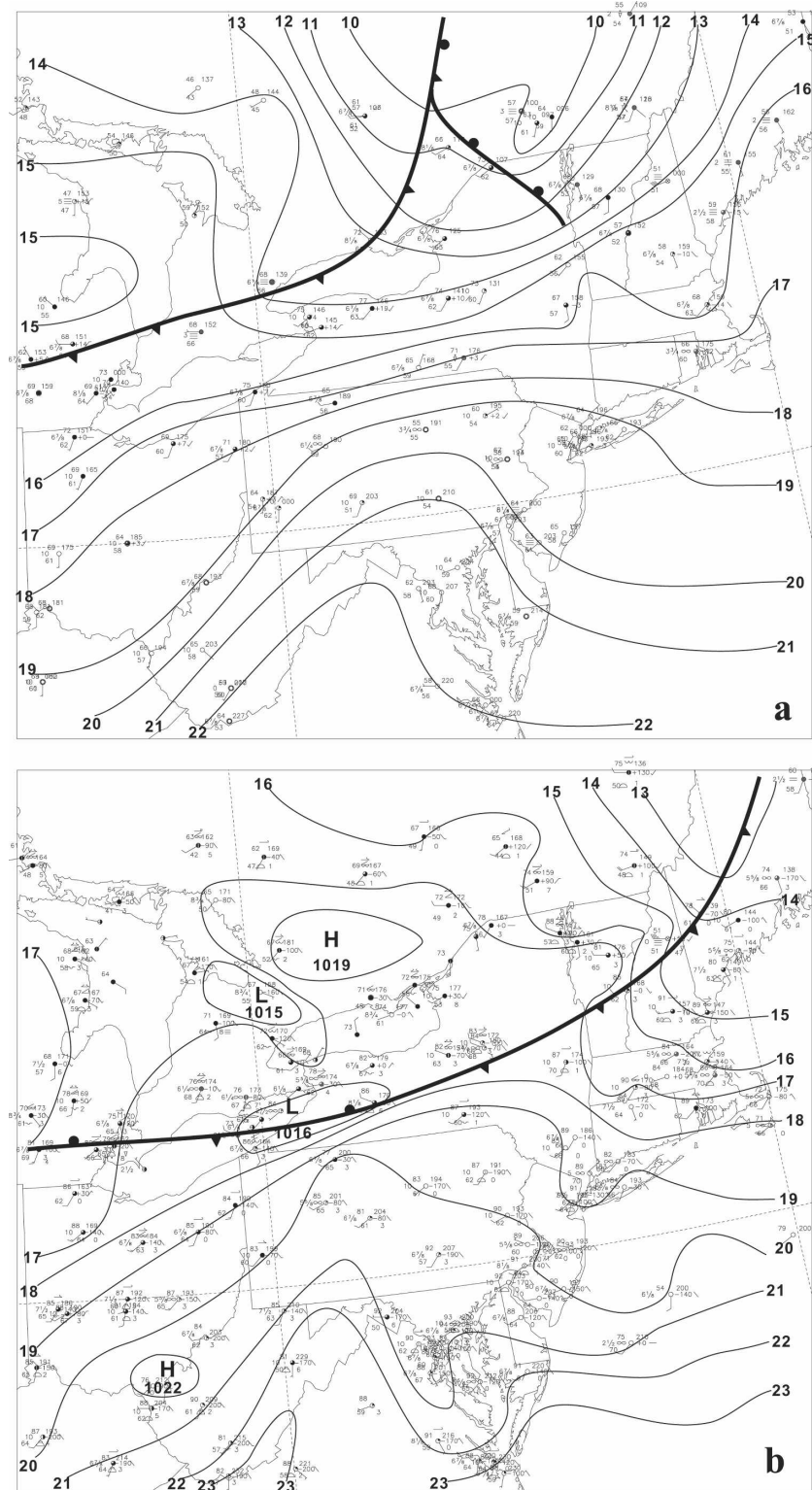


FIG. 2. Standard surface weather analysis at (a) 0900 UTC 19 Sep 1983 and (b) 1800 UTC 19 Sep 1983. Sea level pressure contour interval is 1 hPa. One barb is  $5 \text{ m s}^{-1}$ .

location in space and time. The nudging correction (tendency) defined at a particular grid point depends on the product of the innovation,  $G$ , a horizontal weighting function, a vertical weighting function, and a temporal weighting function (Stauffer and Seaman 1990, 1994). The specific parameters used in this study are defined in the following section.

#### 4. Experimental design

##### a. MM5 configuration

For this study the same grid configuration of 108-, 36-, 12-, and 4-km-resolution domains used in Deng et al. (2004) are used. Details on the horizontal domain sizes and the 32 vertical sigma layers are reported in Deng et al. (2004). The lowest layer is located at about 29 m above ground level (AGL). The thickness of the layers increases gradually with height, with 16 layers below 850 m ( $\sim$ 1560 m AGL). The top of the model is set at 100 hPa. The same initial conditions based on the National Centers for Environmental Prediction global analyses updated by rawinsonde and surface data and used in the previous study (Deng et al. 2004) are used here in the current study. The lateral boundary conditions and three-dimensional (3D) analyses used for Analysis FDDA are defined at 12-h intervals in a way similar to that used for the initial conditions, and surface analysis fields used for surface Analysis FDDA are generated at 3-h intervals. These quality-checked 12-hourly rawinsonde and 3-hourly surface data are also used to create the Obs FDDA fields.

##### b. Model experiments

Because there are no CPSs suitable for the 4-km scale at present, various MM5 sensitivity experiments

are designed to find the best approach to improve the 4-km model simulations. Possible approaches commonly include use of data assimilation. In addition, improved PBL physics, microphysics, and use of an existing CPS on the 4-km grid are also investigated. Because the PBL physics used in mesoscale models ignores horizontal mixing, enhanced horizontal numerical diffusion is also considered. The resulting set of 14 MM5 experiments at 4-km resolution is summarized in Table 1. The first experiment (MB1) is a baseline experiment, which is designed to be identical to experiment 3A in the original study (Deng et al. 2004), except that it uses version 3.6 of MM5, including updated versions of its model physics and its model initialization software. No FDDA is used on the 4-km grid, but Analysis FDDA is used on the outer three grids. No CPS is used on the 4-km grid, but the KF convection scheme is used on the outer grids. The PSU GS PBL scheme and simple ice microphysics are included in the baseline on all four domains, along with the slab force–restore land surface scheme, which includes the radiative effects of the RRTM longwave radiation and Dudhia shortwave radiation schemes in the atmosphere.

The next two FDDA experiments (MB1FA and MB1FO) are configured to be similar to experiment MB1, except that they apply Analysis FDDA and Obs FDDA, respectively, to the 4-km-resolution domain. These experiments are designed to reveal if the lack of FDDA on the 4-km-resolution domain and the potential for greater phase errors in the frontal location contributed to the poorer 4-km results. The 12-km 3D and surface analyses were interpolated to the 4-km-resolution domain for experiment MB1FA and were assimilated the same way as on the 12-km-resolution domain.

TABLE 1. Summary of 4-km-resolution-domain experimental design. Experimental naming convention: MB1: baseline experiment; MB2: baseline experiment using modified GS PBL; FA: Analysis FDDA; FO: Obs FDDA; MRF: MRF PBL instead of GS TKE; KF: Kain–Fritsch CPS; GR: Grell CPS; DIF: enhanced diffusion; MP: mixed-phase microphysics instead of simple ice.

Expt name	PBL physics	CPS	Microphysics	Enhanced vertical mixing	Enhanced diffusion	MM5 FDDA
MB1	GS TKE	None	Simple ice	None	None	None
MB1FA	GS TKE	None	Simple ice	None	None	Analysis FDDA
MB1FO	GS TKE	None	Simple ice	None	None	Obs FDDA
MB2	GS TKE	None	Simple ice	Modified GS TKE	None	None
MB2MRF	MRF	None	Simple ice	Not applicable	None	None
MB2MP	GS TKE	None	Mixed phase	Modified GS TKE	None	None
MB2KF	GS TKE	KF	Simple ice	Modified GS TKE	None	None
MB2DIF1	GS TKE	None	Simple ice	Modified GS TKE	$2 \times K_{H0}$	None
MB2DIF2	GS TKE	None	Simple ice	Modified GS TKE	$5 \times K_{H0}$	None
MB2DIF3	GS TKE	None	Simple ice	Modified GS TKE	$5 \times$ Def	None
MB2DIF3R	GS TKE	None	Simple ice	Modified GS TKE	$5 \times$ Def if rain	None
MB2KFFO	GS TKE	KF	Simple ice	Modified GS TKE	None	Obs FDDA
MB2GRFO	GS TKE	Grell	Simple ice	Modified GS TKE	None	Obs FDDA
MB2MRFGRFO	MRF	Grell	Simple ice	Not applicable	None	Obs FDDA

TABLE 2. Summary of Analysis FDDA coefficients  $G$  ( $10^{-4}$   $s^{-1}$ ). Note that 12-hourly 3D Analysis FDDA of all variables is set to zero in the lowest 1 km AGL and that 3-hourly surface Analysis FDDA using surface-layer wind corrections is applied within the model-diagnosed PBL. See section 4 for details.

MM5 variable	Horizontal grid resolution			
	108 km	36 km	12 km	4km
Wind	2.5	2.5	1.0	1.0
Temperature	2.5	2.5	1.0	1.0
Moisture	0.1	0.1	0.1	0.1

As summarized in Table 2, the Analysis FDDA coefficients for the 12-hourly 3D wind and temperature fields based on rawinsonde data are set to  $G = 2.5 \times 10^{-4} s^{-1}$  on the 108- and 36-km grids and to  $G = 1 \times 10^{-4} s^{-1}$  on the 12- and 4-km domains. Gridded analysis values used in the Analysis FDDA are temporally interpolated to the current model time step. In experiment MB1FA, 3-hourly surface analyses of wind are assimilated throughout the model-diagnosed PBL with the aforementioned nudging coefficient values for each grid and a horizontal weighting function based on the surface data density (Stauffer et al. 1991). No mass fields are used in the surface Analysis FDDA. Although Analysis FDDA is not generally recommended for a 4-km-resolution domain as discussed by Stauffer and Seaman (1994), and especially when only conventional data are available, experiment MB1FA does include Analysis FDDA on the 4-km domain because it was applied on the 12-km domain with  $G = 1 \times 10^{-4} s^{-1}$ . Because rawinsonde moisture fields are too smooth owing to the coarse rawinsonde resolution, which can cause damage to the model quantitative precipitation forecast (QPF), Analysis FDDA of 3D moisture uses a relatively small nudging coefficient  $G = 1 \times 10^{-5} s^{-1}$ . Because only conventional rawinsonde data were used in this study, the 3D analysis nudging coefficients were set to zero below  $\sim 850$  hPa to allow the model to produce finescale structures not resolved by the rawinsonde network.

Experiment MB1FO is configured to be identical to experiment MB1FA, except that it uses Obs FDDA on the 4-km domain for wind, temperature, and mixing ratio. By default, the mass fields are not assimilated in the model-diagnosed PBL because of the poor 12-hourly temporal resolution of the standard rawinsonde network data. The surface observations are assimilated at the surface and within the lowest 250 m AGL using a terrain-dependent nonisotropic weighting function with a maximum radius of influence of 67 km, and upper-air observations are spread quasi horizontally above the surface with an isotropic influence function

with a radius of influence that varies from 100 km just above the surface to 200 km at 500 hPa, held constant up to the model top (Stauffer and Seaman 1994). Observations are assimilated using the temporal weighting function defined by Stauffer and Seaman (1994) over a time window with a half-period of 120 (60) min on each side of the observation time for upper-air (surface) data. The Obs FDDA coefficients are set to  $G = 4 \times 10^{-4} s^{-1}$ . This experiment is to evaluate the effectiveness of Obs FDDA in this CAPTEX-83 case and to compare this technique with the Analysis FDDA, especially in the PBL. This approach is generally more appropriate for use on finer-resolution domains than is Analysis FDDA.

Experiment MB2 is identical to the baseline, except that it includes some changes to the vertical mixing length scales in the GS PBL scheme to increase the parameterized mixing. Recent experimentation at PSU, including extensive U.S. Army testing of its MM5 system based in a high-mobility multipurpose wheeled vehicle (HMMWV, also known as “humvee”; Schroeder et al. 2006; Stauffer et al. 2004), has shown improvements in PBL structure when increasing the parameterized mixing lengths in the GS PBL. Experiment MB2 uses 50% larger mixing lengths and eddy diffusivity  $K$  in the first layer above the surface layer and double the default values above this layer. Because this enhanced parameterized vertical mixing in the GS PBL scheme produced improved model simulations on the 4-km grid, these improvements were adopted for all GS PBL sensitivity experiments from this point forward, and therefore experiment MB2 may be considered a new baseline experiment. No FDDA is used on the 4-km grid.

Experiment MB2MRF is identical to the baseline MB1 except that the MRF PBL scheme is used. This experiment is to evaluate the effect of a different turbulence (PBL) scheme and its impact on the grid-resolved convection at 4-km resolution. No FDDA is used on the 4-km grid.

Experiment MB2MP is identical to experiment MB2 except that it is designed to investigate the impact of mixed-phase microphysics on the 4-km cloud, precipitation, and flow fields. In this experiment both ice and liquid can coexist in a given grid cell, and the hydrometeor type and its fall velocity can influence the intensity of the downdraft, the cold pool, and, thus, the low-level wind patterns. No FDDA is used on the 4-km grid.

Experiment MB2KF is designed to investigate the use of the KF convective parameterization on the 4-km domain to release the CAPE gradually, thereby reducing the intensity of the grid-resolved convection. Note that use of a CPS at 4-km resolution may violate its

underlying assumption that the parameterized subgrid process is much smaller than the grid cell (e.g., Arakawa and Schubert 1974). No FDDA is used on the 4-km grid. Because the aforementioned PBL schemes lack horizontal mixing, several experiments are designed to investigate the MM5 sensitivity to enhanced horizontal diffusion and its effect on the gridpoint storms. Note that the simulated updrafts and down-drafts on a 4-km grid are occurring on scales that are generally larger than those found in nature in the northeastern United States. There are no physically realistic lateral (horizontal) mixing processes in MM5 to dilute the 4-km updraft, however. The turbulence schemes used in mesoscale models were originally developed for scales on which the horizontal mixing effects are much smaller than the vertical mixing effects and therefore can be ignored. As resolutions approach 1–5 km or so, however, the lateral mixing across, say, a cloud boundary may be important and should be included. Additional terms are actually needed, such as those involving the horizontal gradients of vertical motion. These terms are typically found in the three-dimensional subgrid turbulence schemes within a large eddy simulation or cloud-scale model; the enhanced horizontal diffusion here is intended to emulate these terms.

The Smagorinsky horizontal diffusion in MM5 (based on the sum of a constant background term and a term based on the horizontal deformation field) can be adjusted to increase further the numerical smoothing and thus to emulate in a crude way the entrainment and detrainment of a moist updraft. The horizontal diffusion coefficient in MM5 can be given by

$$K_H = K_{H0} + C \times \text{Def}, \quad (1)$$

where  $K_{H0}$  is a background value of the diffusion coefficient, with a default value of  $4 \times 10^3 \text{ m}^2 \text{ s}^{-1}$  for the 4-km grid,  $C$  is a dimensional constant, with a default value of 160 m for the 4-km grid, and  $\text{Def}$  is the deformation term (Smagorinsky et al. 1965). Experiment MB2DIF1 uses exactly the same configuration as experiment MB2 does, except that it uses a doubled background horizontal diffusion coefficient  $K_{H0}$  in Eq. (1). Experiment MB2DIF2 is identical to experiment MB2DIF1 except that it uses a background horizontal diffusion coefficient that is 5 times the default value used for experiment MB2. Experiment MB2DIF3 is the same as MB2DIF1 except that it increases the deformation term in Eq. (1) by 5 times while keeping the original default background term (experiment MB2) to investigate how enhanced diffusion determined by the deformation field affects the MM5 simulations on the 4-km grid. Experiment MB2DIF3R is identical to experiment MB2DIF3 except that it only applies the en-

hanced diffusion through the deformation term on the grid cells where precipitation occurred in the previous time step, with a threshold precipitation value of  $1 \times 10^{-6} \text{ cm}$ . This last experiment addresses the potentially adverse effects of increased horizontal smoothing on model-generated mesoscale circulations by limiting its use to areas experiencing precipitation and where gridpoint storms are more likely. No FDDA is used on the 4-km grid for these diffusion experiments.

Experiments MB2KFFO, MB2GRFO, and MB2MRFGRFO investigate the value of Obs FDDA when combined with a CPS on the 4-km domain. Experiment MB2KFFO is identical to MB2 except that it applies KF to the 4-km grid along with Obs FDDA. It uses default values for the horizontal diffusion coefficient and the enhanced vertical mixing in the GS PBL scheme as used in MB2. Experiment MB2GRFO is identical to experiment MB2KFFO except that the Grell CPS is used on all domains, including the 4-km domain, in lieu of KF. Experiment MB2MRFGRFO uses another commonly used physics combination—the MRF PBL and the Grell CPS—on all domains (e.g., Zhong and Fast 2003; Tan et al. 2004), along with Obs FDDA on the 4-km-resolution domain only.

## 5. Model results

Evaluation of simulated meteorological features is accomplished by subjectively comparing the model's 4-km QPF and surface meteorological fields to the observed surface maps and satellite images. Because the spatial distribution and amount of precipitation may be very different between the simulation and the limited observations, objective validation of precipitation is generally very difficult. Objective evaluation is performed by comparing the statistical scores of the model-simulated wind speed, wind direction, vector wind difference, temperature, water vapor mixing ratio, and sea level pressure, which all reflect to some degree the skill in QPF.

### a. Subjective evaluation of the MM5-simulated mesoscale features

Although the simulated fields at all model times have been carefully examined, the focus for this section is placed on presenting the precipitation fields and relevant surface meteorological fields at two model times: 0900 UTC 19 September 1983 (21 h) and 1800 UTC 19 September 1983 (30 h). The 21-h time represents local nighttime conditions and anomalous surface winds associated with excessive precipitation ahead of the cold front in the Lake Erie region. The 30-h time represents daytime conditions when the 4-km MM5 results re-

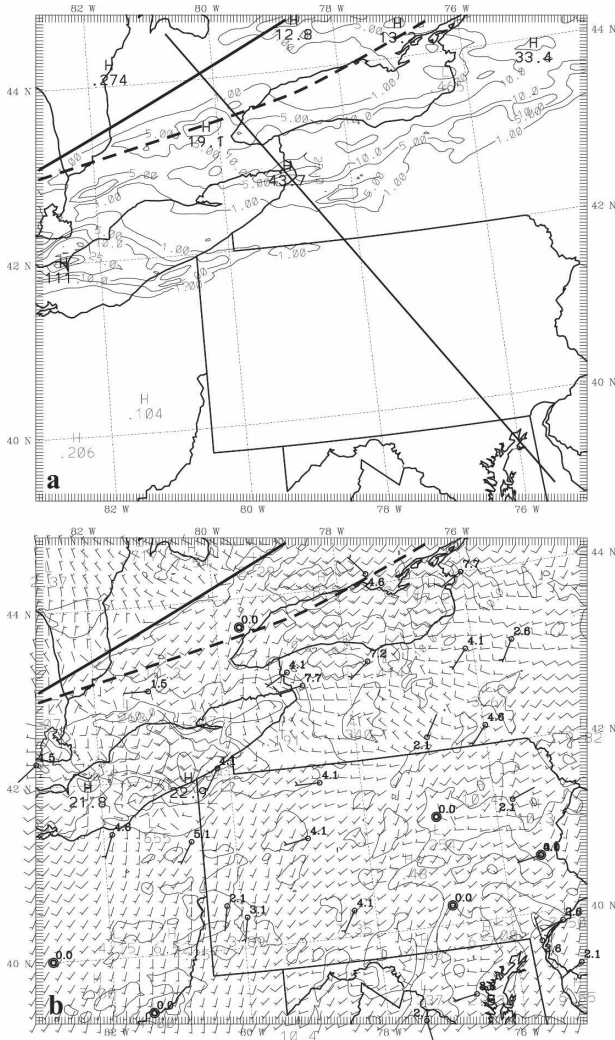


FIG. 3. MM5-simulated field at 21 h (0900 UTC 19 Sep 1983) on the 4-km-resolution domain in expt MB2 for (a) 3-h total rainfall (mm), with contours of 1, 5, 10, and 25 mm, and (b) surface-layer wind (29 m AGL) overlaid with observed surface winds. Speed contours are  $5 \text{ m s}^{-1}$ , and one barb is  $10 \text{ m s}^{-1}$ . The observed (dashed) and simulated (solid) fronts are shown on the figure for reference. The northwest-southeast line indicates the location of the cross section used in Fig. 4.

ported by Deng et al. (2004) reflected a spurious mesoscale convective system in the northwestern Pennsylvania–southwestern New York area.

### 1) 21-H MODEL TIME

At 0900 UTC 19 September 1983 (21 h), although the mesoscale features of the precipitation fields are somewhat different from one experiment to another, all experiments in Table 1 produce a banded structure of heavy precipitation associated with the front (e.g., experiment MB2 in Fig. 3a). Examination of the wind

field at the lowest model layer indicates that the simulated frontal positions for each experiment are quite similar, and they are generally slower than the observed front (e.g., Fig. 3b). As indicated by Deng et al. (2004), slower-than-observed phase speeds are known to be a general characteristic of finite-difference models.

Experiment MB1 has a widespread precipitation pattern ahead of the model-simulated cold front, with a maximum value of 108 mm over Lake Erie resulting from a gridpoint storm (not shown). This QPF is surely much larger than observed for this 3-h period based on the observed 24-h total precipitation included in Table 3. When FDDA is applied on the 4-km-resolution domain, Table 3 shows that both experiments MB1FA and MB1FO reduce the erroneous maximum value of precipitation over Lake Erie by about 25% and that the rainband associated with the cold front has narrowed somewhat (not shown) and has become more organized. The convective precipitation area still appears to be overpredicted from Lake Erie extending to the northeast along the front, however.

Figure 3a shows the model-simulated 3-h precipitation field ending at 21 h for experiment MB2. Although significant improvements in the precipitation field in experiment MB2 may not be readily apparent, with the 111-mm maximum still located in southern Lake Erie, more realistic mixed-layer profiles of mixing ratio (not shown) and improvements in the statistical scores (section 5) suggest that the modified length scales in the GS PBL be adopted for all other GS PBL sensitivity experiments. It is shown that the Lake Erie precipitation

TABLE 3. Model-simulated maximum 3-h precipitation (mm) and maximum surface wind speed ( $\text{m s}^{-1}$ ) over the Lake Erie precipitation region ahead of the cold front for 21 h (0900 UTC 19 Sep 1983). The last row of the table shows observed 24-h total precipitation and average wind speeds based on available land observations near the lake.

Expt name	Max 3-h precipitation	Max surface wind speed
MB1	108.0	20.0
MB1FA	74.4	15.1
MB1FO	78.5	20.0
MB2	111.0	21.8
MB2MRF	0.0	—
MB2MP	92.7	18.2
MB2KF	62.0	16.9
MB2DIF1	123.0	17.3
MB2DIF2	111.0	22.0
MB2DIF3	94.0	22.0
MB2DIF3R	118.0	19.9
MB2KFFO	55.0	14.2
MB2GRFO	42.6	14.4
MB2MRFGRFO	47.2	14.2
OBS	<0.5	~5.0

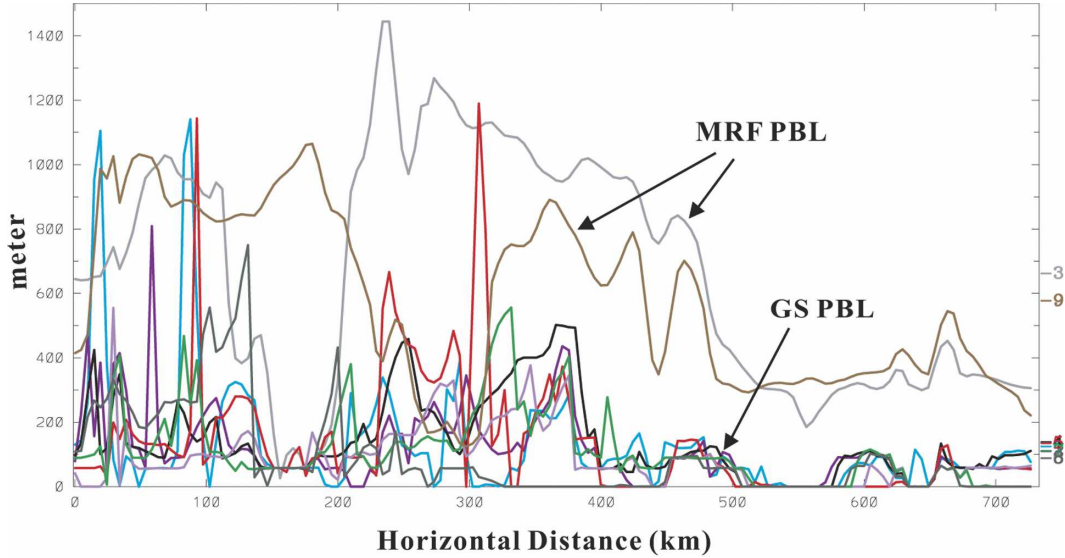


FIG. 4. MM5-simulated PBL height along the northwest-southeast cross section shown in Fig. 3a for all experiments on the 4-km-resolution domain at 21 h (0900 UTC 19 Sep 1983). The cross-sectional mean PBL height values are plotted on the side of the chart with the digital values also included above the experiment key at the bottom of the figure.

area, which is located in the warm sector ahead of the cold front, is clearly defined by the surface wind convergence zone in Fig. 3b. A very strong southwesterly wind speed of  $21.8 \text{ m s}^{-1}$  is found near the precipitation region. Away from the region of disturbed weather over Ohio and Pennsylvania, the model and observed surface winds show good agreement.

Table 3, which summarizes the model-simulated maximum precipitation and surface winds over the Lake Erie region for this time, shows that both baseline experiments (experiments MB1 and MB2) produce gridpoint storms with 3-hourly precipitation amounts exceeding 100 mm and wind speeds greater than  $20 \text{ m s}^{-1}$  over Lake Erie. In experiment MB2MRF, in which the MRF PBL scheme is used, the aforementioned precipitation pattern over Lake Erie that existed in other experiments has completely disappeared (not shown). This total lack of precipitation in this southern Lake Erie region by experiment MB2MRF is not consistent with the surface observations or satellite imagery or with any of the other experiments using the GS PBL scheme. The zero precipitation may be related to the larger vertical mixing associated with the much deeper PBL heights produced by the MRF scheme in this region, even during the night (Fig. 4), in comparison with the experiments using the GS PBL. Note that the average PBL height along the cross section in Fig. 4

for experiments using the MRF PBL (experiments MB2MRF and MB2MRFGRFO) is larger than that in the other experiments by a factor of 3–4.

In experiment MB2MP, which uses mixed-phase microphysics, maxima of 92.7 mm and  $18.2 \text{ m s}^{-1}$  are still located over Lake Erie, but, as compared with experiment MB2, it has a banded precipitation pattern that shows enhanced and more localized precipitation in some regions (not shown). There appears to be smaller areal coverage of lighter precipitation amounts and more concentrated coverage of the higher precipitation amounts. This result may be explained by the fact that mixed-phase microphysics allows more ice particles, and they do not advect as far from the updraft as liquid drops because of their higher fall speeds, so that the precipitation becomes more localized.

When the KF scheme is applied on the 4-km-resolution domain, experiment MB2KF shows reduced areal coverage in the precipitation pattern relative to MB2, the Lake Erie total precipitation maxima is reduced to 62.0 mm, and the associated wind maximum has weakened to  $16.9 \text{ m s}^{-1}$ . The experiment-MB2KF maximum precipitation (convective plus explicit) values are generally smaller than those in experiment MB2, and the areal coverage is somewhat reduced and is more consistent with the cloud band that was observed at 0830 UTC 19 September 1983 (not shown).

The convective scheme appears to release some of the CAPE so that the explicit scheme response is now much weaker in magnitude and areal coverage. The experiment-MB2KF explicit maximum over Lake Erie is about 50% of that in MB2 (52.5 vs 111 mm), and the total MB2KF rain maximum is slightly higher than the explicit value at 62.0 mm.

Several experiments use enhanced horizontal diffusion in an attempt to reduce the spurious explicit QPF. In experiments MB2DIF1 and MB2DIF2 the baseline background diffusion is increased by a multiplication factor of 2–5. Experiment MB2DIF3 applies a fivefold increase in smoothing through the deformation term, whereas experiment MB2DIF3R does so only where it was raining at the previous time step. The results of these diffusion experiments are very similar and still overestimate localized precipitation. In fact, two of the experiments produce even larger precipitation amounts than the baseline MB2 (Table 3). Therefore, they have little impact on reducing the excessive precipitation amounts at this time. Thus, use of larger horizontal diffusion as a solution to this gridpoint storm problem appears to be ineffective. The simulated maximum surface wind speeds are also still very large (17.3–22.0 m s<sup>-1</sup>).

Combining a CPS and Obs FDDA on the 4-km-resolution domain in experiments MB2KFFO, MB2GRFO, and MB2MRFGRFO produces the largest reduction in the total maximum precipitation (~50%) and the surface wind speed maximum (~35%) for the Lake Erie region relative to those of the baseline MB2, although the maxima are still seriously overestimated. The experiment-MB2KFFO precipitation pattern is very similar to that in experiment MB2 (Fig. 3a). Experiments MB2GRFO and MB2MRFGRFO, which use Grell CPS, produce much greater convective precipitation coverage over Ohio and New York, however, and these results are not supported by the surface map (Fig. 2a) and satellite photo (not shown) at this time.

## 2) 30-H MODEL TIME

As discussed in Deng et al. (2004), the observed surface conditions at 1800 UTC 19 September 1983 (30 h) over the 4-km-resolution domain show no reported precipitation. There is observed southwesterly flow at the surface through most of Ohio and Pennsylvania (Fig. 2b). The satellite photo at this time (not shown) confirms the absence of significant clouds over Pennsylvania and southern New York. The 4-km domain experiment 3A in the previous study by Deng et al. (2004) and 4-km experiment MB1 in this study produce a mesoscale convective system (not shown) ahead of the front in northwest Pennsylvania with divergent low-level

flow seriously disrupting the southwesterly flow at the surface and a cold pool in the surface temperature field. The maximum amount of model-simulated 3-h precipitation for experiment MB1 at 30 h is 66.5 mm located in northwestern Pennsylvania, associated with outflow boundaries and a cold-pool temperature of 17.0°C and a mesohigh of 1022 hPa (see Table 4). As discussed in Deng et al. (2004), the primary cause of the poor mesoscale model performance was likely the explicit (grid resolved) representation of convection. Because no CPS is used on the 4-km grid in experiment MB1, the convective updrafts are forced on coarser-than-realistic scales (normal updraft diameter for most storms in the eastern United States is ~2 km), and the rainfall and the atmospheric response to the convection are too strong. The evaporative cooling and the associated downdrafts are too vigorous, causing widespread disruption of the low-level winds.

In experiment MB2 in which turbulence mixing-length scales and coefficients are modified in the GS PBL scheme, although the simulated precipitation patterns at 30 h (Fig. 5a) are similar to experiment MB1, the maximum values of precipitation in experiment MB2 are reduced from 66.5 to 56.7 mm in northwestern Pennsylvania. Associated with the precipitation field at this time, there is a clear divergent pattern (outflow boundaries) in the simulated surface wind field (Fig. 5b), a cold pool (17.5°C) in the simulated surface temperature field (Fig. 5c), and a mesohigh (1020 hPa) in the simulated sea level pressure field (Table 4). It is apparent that enhancing the vertical mixing does not

TABLE 4. Model-simulated maximum 3-h total precipitation (mm), minimum cold-pool temperature (°C), and mesohigh pressure value (hPa) associated with the mesoscale convective system precipitation pattern at 30 h (1800 UTC 19 Sep 1983) over the 4-km-resolution domain for each experiment. The last row of the table shows observed 24-h total precipitation.

Expt name	3-h precipitation (mm)	Cold-pool temperature	Cold-pool pressure
MB1	66.5	17.0	1022
MB1FA	53.3	18.0	1019
MB1FO	21.9	18.3	1018
MB2	56.7	17.5	1020
MB2MRF	51.7	16.1	1022
MB2MP	88.6	18.0	1020
MB2KF	3.9	—	—
MB2DIF1	23.6	19.3	1016
MB2DIF2	11.1	18.7	1018
MB2DIF3	22.3	17.9	1016
MB2DIF3R	37.9	18.0	1016
MB2KFFO	11.7	—	—
MB2GRFO	0.6	—	—
MB2MRFGRFO	1.2	—	—
OBS	<0.5	—	—

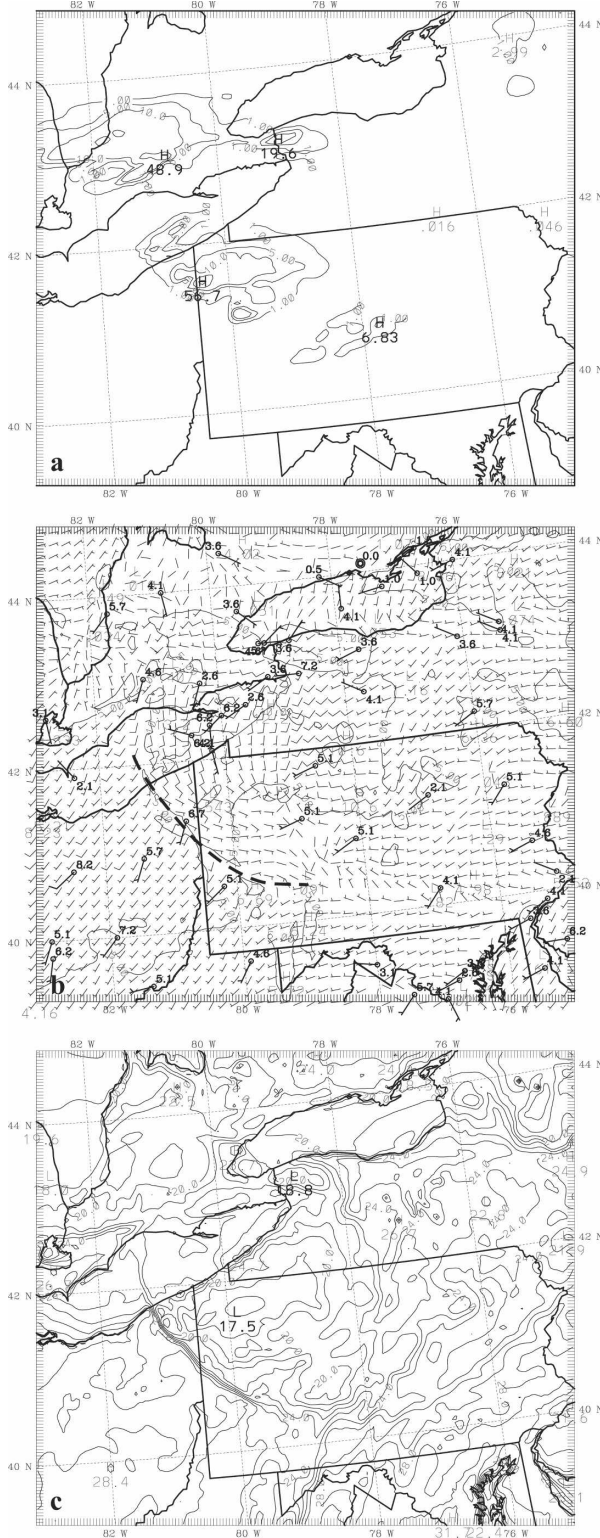


FIG. 5. MM5-simulated fields at 30 h (1800 UTC 19 Sep 1983) on the 4-km-resolution domain in expt MB2: (a) 3-h total rain, (b) surface-layer wind (29 m AGL) overlaid with observed surface winds, and (c) surface-layer temperature. Rain contours are 1, 5, 10, and 25 mm, speed contours are  $5 \text{ m s}^{-1}$  and one barb is  $10 \text{ m s}^{-1}$ , and temperature contours are  $2^\circ\text{C}$ . Dashed line in (b) indicates a wind-shift line related to the outflow boundary.

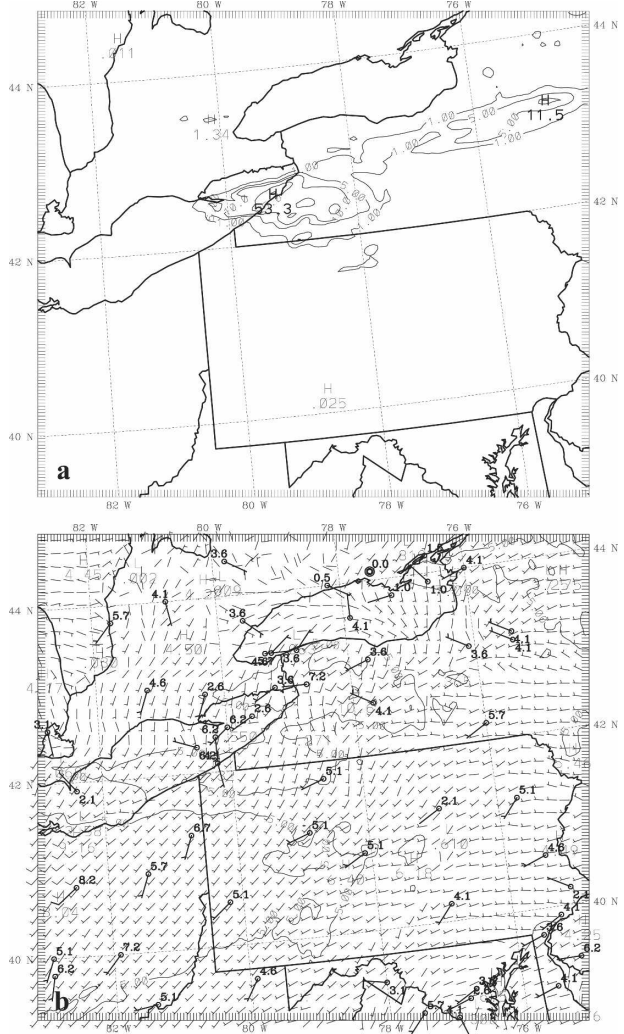


FIG. 6. MM5-simulated fields at 30 h (1800 UTC 19 Sep 1983) on the 4-km-resolution domain in expt MB1FA: (a) 3-h total rain and (b) surface-layer wind (29 m AGL) overlaid with observed surface winds. Rain contours are 1, 5, 10, and 25 mm, speed contours are  $5 \text{ m s}^{-1}$  and one barb is  $10 \text{ m s}^{-1}$ , and temperature contours are  $2^\circ\text{C}$ .

solve the problem with excessive gridpoint convection on the 4-km-resolution domain when no CPS is applied.

When FDDA is applied on the 4-km grid, both precipitation amount and the areal coverage at 30 h are reduced in comparison with experiment MB1 (not shown). In experiment MB1FA in which Analysis FDDA is used, precipitation appears in southern New York with a maximum amount of 53.3 mm (Fig. 6a). Surface wind fields (Fig. 6b) do not show a divergent pattern in northwest Pennsylvania, but there are anomalous winds over Lake Erie. The surface temperature field shows a cold pool ( $18.0^\circ\text{C}$ ) and the sea level pressure field shows a weaker mesohigh (1019 hPa) as-

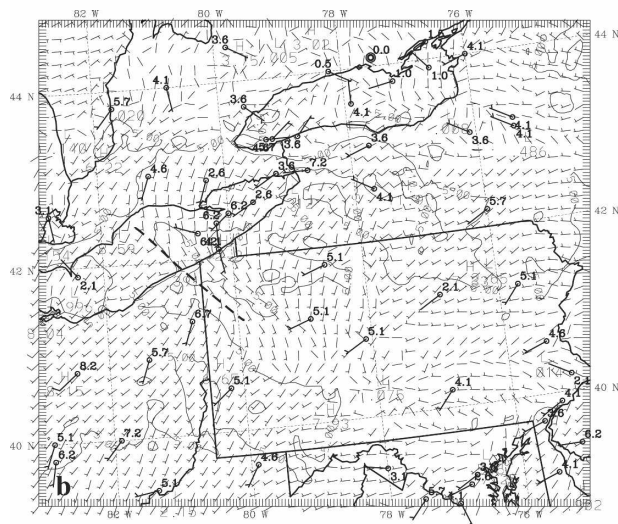
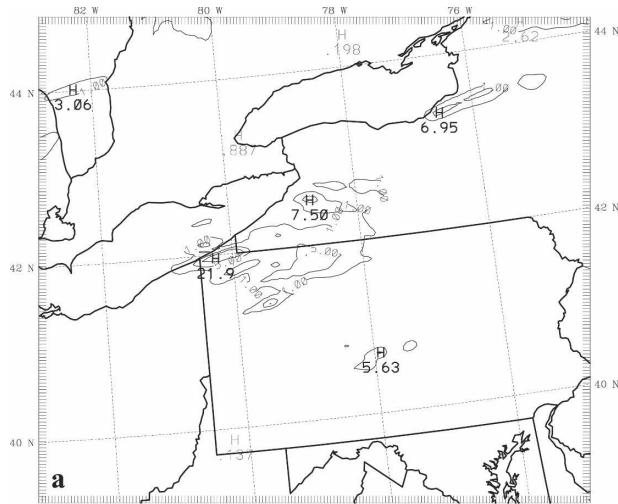


FIG. 7. As in Fig. 6, but for expt MB1FO.

sociated with the precipitation in southern New York near Lake Erie (see Table 4). In experiment MB1FO in which Obs FDDA is used, the simulated 3-h precipitation ending at 30 h (Fig. 7a) is reduced in magnitude relative to that of experiment MB1FA in northwestern Pennsylvania near Lake Erie, with a maximum value of 21.9 mm as compared with experiment MB1FA at 53.3 mm (Fig. 6a). In a similar way, the surface wind field for experiment MB1FO at this time (Fig. 7b) does not show any strong divergence, although the winds have turned to southerly or even southeasterly in northwest Pennsylvania where the temperature field is locally cooler ( $18.3^{\circ}\text{C}$ ).

When the MRF PBL scheme is used in lieu of the GS PBL scheme in experiment MB2MRF, MM5 has produced a significantly worse simulation in the model-simulated precipitation field at 30 h (Fig. 8a) than that

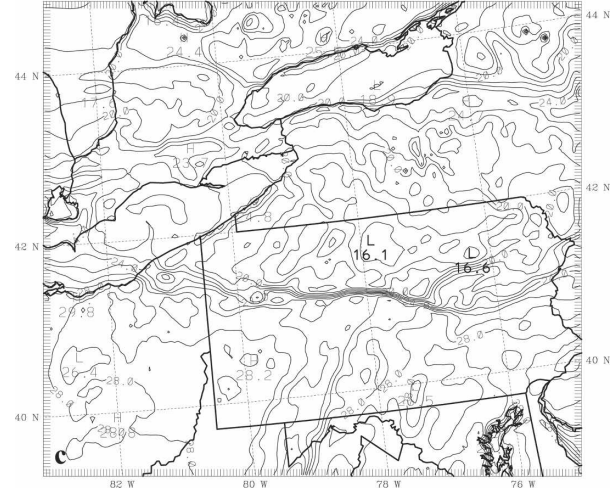
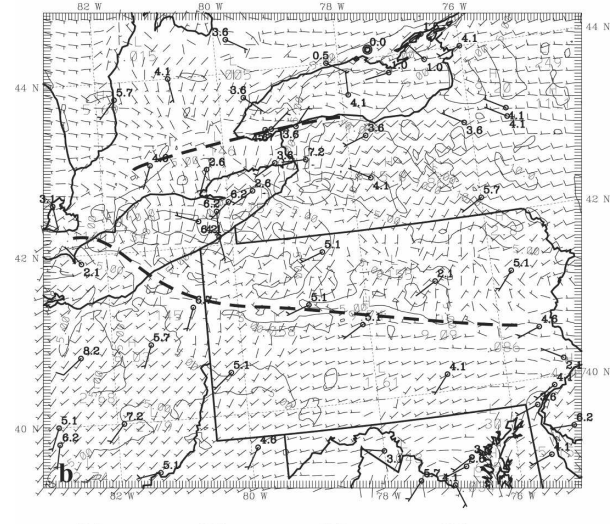
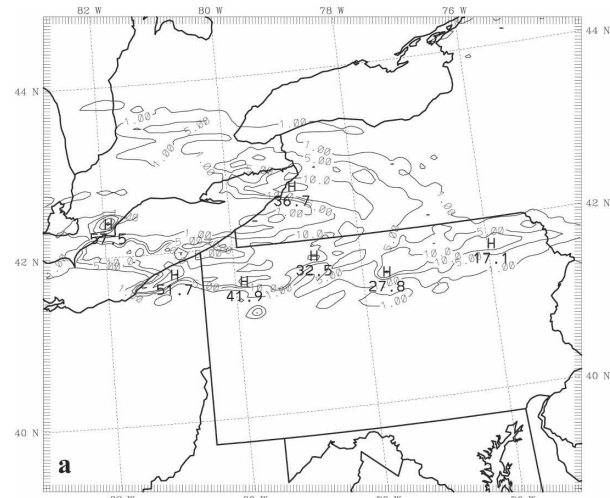


FIG. 8. As in Fig. 5, but for expt MB2MRF.

in experiment MB1 because the spurious convection has spread to a much larger area, covering a portion of Lake Erie and the entire northern third of Pennsylvania. The simulated surface wind field at 30 h (Fig. 8b) also shows an even larger area of disturbed flow with outflow boundaries. The simulated surface temperature field at 30 h (Fig. 8c) indicates a much broader area of cold pools across northern Pennsylvania, with colder minimum temperatures of  $16.1^{\circ}$  and  $16.6^{\circ}\text{C}$  and a mesohigh of 1022 hPa embedded within the evaporatively cooled air across northern Pennsylvania (Table 4). Therefore, experiment MB2MRF greatly increases the magnitude and coverage of the erroneous rain and anomalous surface meteorological conditions at this time. Analysis of PBL depth at this time (not shown) indicates that the MRF scheme produces much deeper unrealistic simulated PBL heights. The stronger vertical mixing associated with the MRF scheme is producing much different and worse QPF. The MRF scheme appears to introduce significant error in this case.

Figure 9a shows the simulated MB2DIF2 precipitation field at 30 h. It is shown that the maximum amount of precipitation over the Lake Erie region has been reduced to 11.1 mm and the entire area of the precipitation has also been reduced relative to that in MB2, and the simulated surface wind field (Fig. 9b) at 30 h is more southwesterly in western Pennsylvania but still shows an anomalous wind pattern located in southwestern New York. A cold pool of  $18.7^{\circ}\text{C}$  is located over the Lake Erie region (Table 4). The rest of the diffusion experiments have similar results, with somewhat smaller precipitation amounts than that in experiment MB2, although there are cold pools and mesohighs associated with the precipitation patterns (Table 4). These results show that use of larger horizontal diffusion alone as a solution to this gridpoint-storm problem led to some improvement at this time, but, as Table 3 showed, the improvement is not generally true for other times.

Consistent with the 21-h time results, when mixed-phase microphysics is applied in experiment MB2MP, the MM5-simulated precipitation (not shown) tends to cover a smaller area, with even more intense precipitation (88.6 mm) in northeast Ohio and northwest Pennsylvania. Table 4 shows that accompanying the precipitation is a divergent pattern in the simulated surface wind field, which is associated with a cold pool (18.0°C) in the surface temperature field and a mesohigh (1020 hPa) in the sea level pressure field. The areal coverage of precipitation is smaller than that in experiment MB2 (not shown).

When the KF scheme is applied on the 4-km-resolution domain, the experiment-MB2KF total pre-

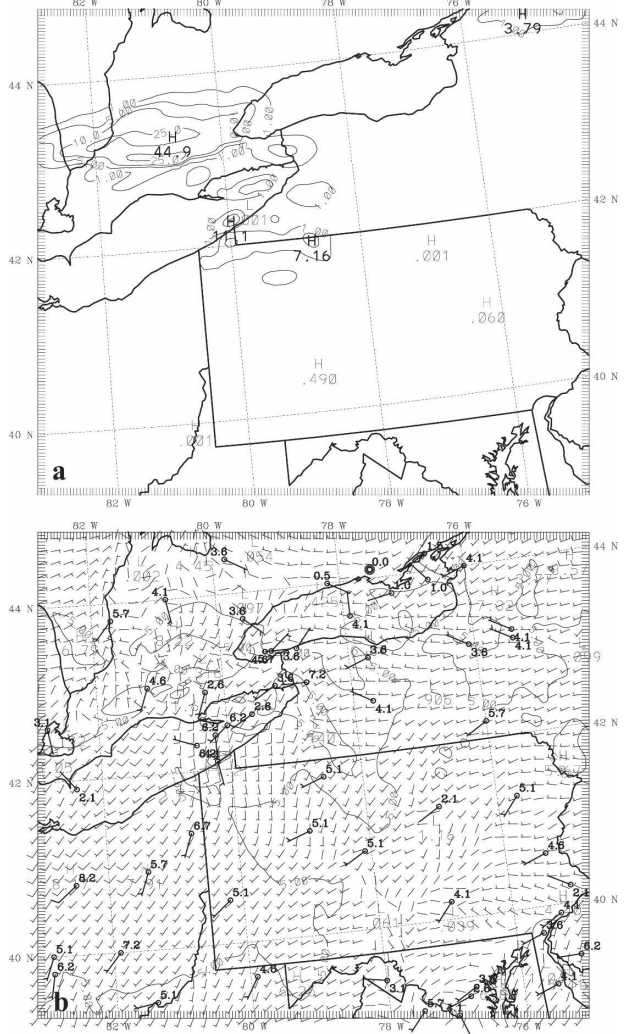


FIG. 9. As in Fig 6, but for expt MB2DIF2.

cipitation shown in Fig. 10a is generally much lighter than that of the other experiments in this region. Experiment MB2KF greatly reduces the nonconvective rain produced by the explicit microphysics, and the convective scheme produces light or no precipitation in northwest Pennsylvania (not shown) where gridpoint-type storms had developed in all of the other experiments (experiments MB1, MB1FA, MB2, MB2MRF, and MB2MP). Examination of the model-simulated surface wind field at 30 h (Fig. 10b) verifies that the MM5 surface winds are much improved by the model not producing the significant precipitation and low-level divergent response to the evaporative cooling. The surface temperature field does not exhibit a cold pool (not shown). Thus, experiment MB2KF produces some very interesting and also positive results on the 4-km-resolution domain by not producing the spurious

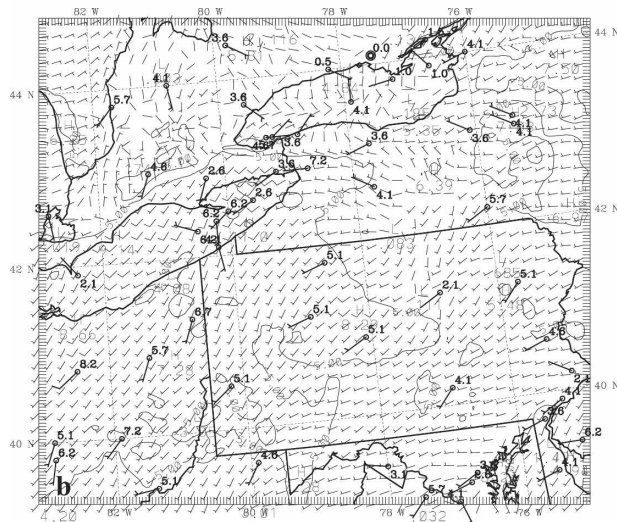
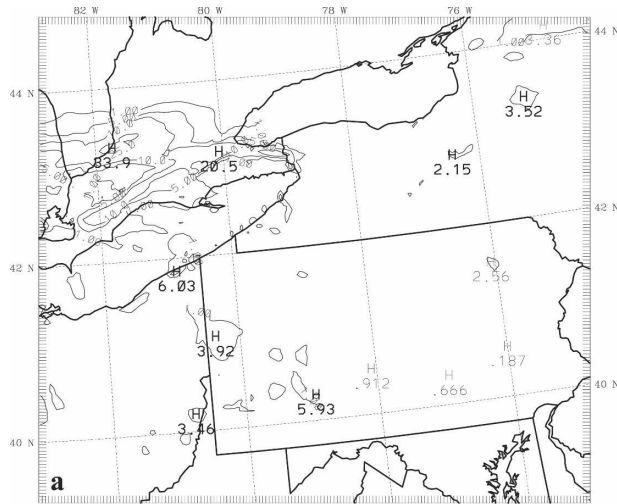
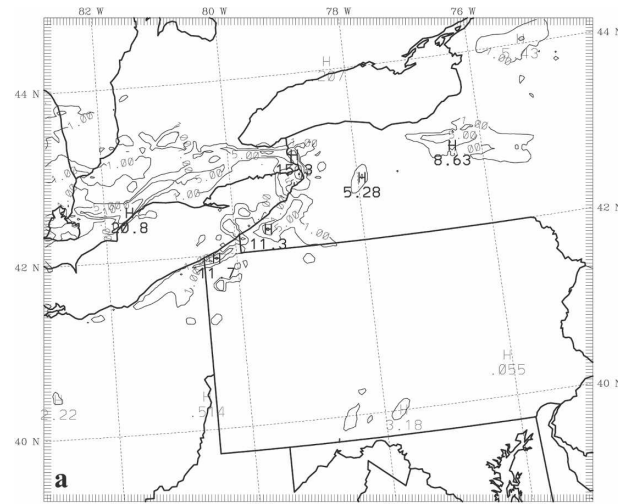


FIG. 10. As in Fig. 6, but for expt MB2KF.

gridpoint precipitation and its adverse effects on the surface wind and mass fields.

Because Obs FDDA and KF have been shown to improve the model solutions, experiment MB2KFFO combines both Obs FDDA and KF on the 4-km-resolution domain. The total precipitation in experiment MB2KFFO (Fig. 11a) covers a slightly larger area than that in MB2KF in southwestern New York, where the precipitation amounts are still generally small. The precipitation is further reduced compared to that of experiment MB2KF in western Pennsylvania. The experiment MB2KFFO surface wind field (Fig. 11b) shows good agreement with the observed southwesterly flow over northwestern Pennsylvania and Lake Erie, with no divergent outflow boundaries and no surface temperature cold pools (not shown).

A different CPS (Grell scheme) is used with Obs



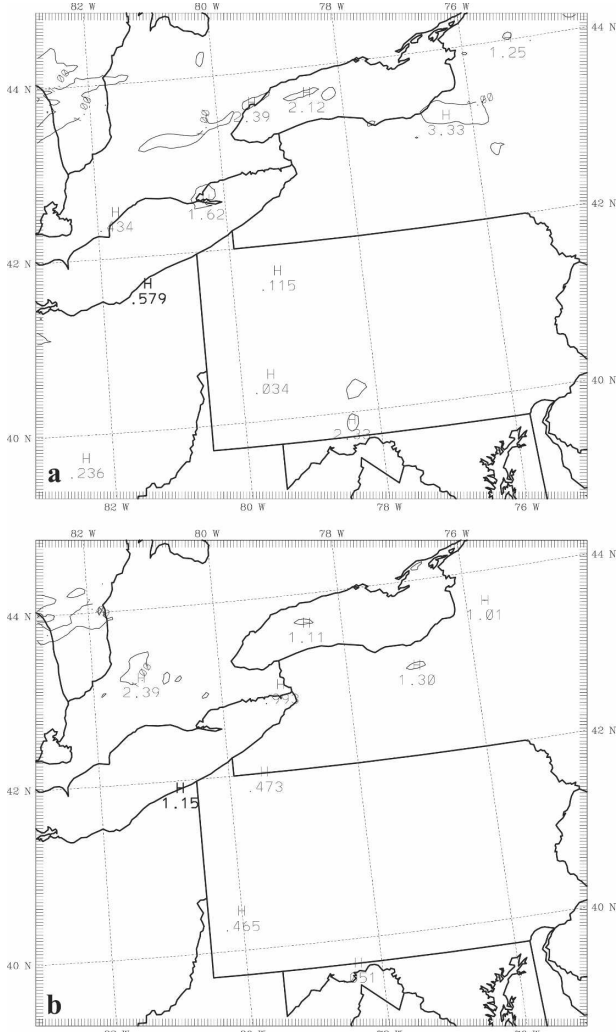


FIG. 12. MM5-simulated 3-h total rain at 30 h (1800 UTC 19 Sep 1983) on the 4-km-resolution domain in expts (a) MB2GRFO and (b) MB2MRFGRFO. Rain contours are 1, 5, 10, and 25 mm.

4 shows the maximum values of the precipitation pattern in northwestern Pennsylvania–southwestern New York near Lake Erie and the associated cold-pool temperatures and mesohigh pressures for all experiments. The table indicates that at 30 h in experiments MB1, MB1FA, MB2, MB2MRF, and MB2MP, the simulated precipitation maxima are very large; and each of these experiments shows an evaporatively induced cold pool in the simulated surface temperature field and locally higher sea level pressures. It is worth mentioning that experiment MB2MRF, which used the MRF PBL scheme, has the coldest and broadest surface cold pool with its minimum of  $16.1^{\circ}\text{C}$  in the higher terrain of north-central Pennsylvania associated with a 27.8-mm precipitation maximum. Experiment MB1FO using Obs FDDA shows lighter precipitation and a cold pool

of  $18.3^{\circ}\text{C}$ . Experiments MB2KF, MB2KFFO, MB2GRFO, and MB2MRFGRFO show much reduced precipitation and no cold pool or mesohigh associated with the precipitation. These experiments appear to produce the best low-level flow pattern at this time, with consistent southwesterly flow across Pennsylvania into southern New York. Thus, use of the combination of Obs FDDA and a CPS on the 4-km-resolution domain produces the most significant positive impact on the model solutions on the 4-km grid in this CAPTEX-83 case. These subjective conclusions will be further investigated using the objective statistical evaluation in the next section.

*b. Objective evaluation of the MM5 solutions using a statistical approach*

Although the statistical measures root-mean-square errors (rmse), mean absolute errors (MAE), mean errors (ME), and index of agreement  $I$  (Willmott et al. 1985) are computed for the MM5-simulated wind and mass fields, only MAE and ME scores are discussed here. The statistics are calculated over the entire 4-km-resolution domain.

1) WIND FIELD

Figure 13 shows vertical profiles of 30-h-averaged MAE of the MM5-simulated wind speed over the entire 4-km-resolution domain. Combining KF with the Obs FDDA on the 4-km domain in experiment MB2KFFO produces the best overall results ( $1.1 \text{ m s}^{-1}$ ) with MB1FO, MB2GRFO, and MB2MRFGRFO close behind and within  $0.1 \text{ m s}^{-1}$ . The profile-averaged values of the statistics are plotted at the top of the figure and are listed above the experiment key at the bottom of the figure. The experiment MB1FA (Analysis FDDA) average error of  $1.6 \text{ m s}^{-1}$  is about halfway between the Obs FDDA experiments and the rest of the experiments around  $2.1 \text{ m s}^{-1}$ .

Experiments MB2KFFO and MB1FO show smaller MAE of wind speed than do MB2GRFO and MB2MRFGRFO in most of the layer below 1.5 km. Experiments MB1FO, MB2GRFO, and MB2MRFGRFO have a small advantage over MB2KFFO in the lowest few layers in the PBL. Therefore, Obs FDDA in particular seems to have the most significant contribution to reducing model errors in wind speed on the 4-km-resolution domain. Note that Analysis FDDA using conventional surface wind analyses in the PBL (experiment MB1FA) does not perform as well in the lowest 1 km as Obs FDDA or the non-FDDA model experiments on this 4-km grid scale. The model error in wind speed for experiment MB1FA in Fig. 13 is significantly reduced

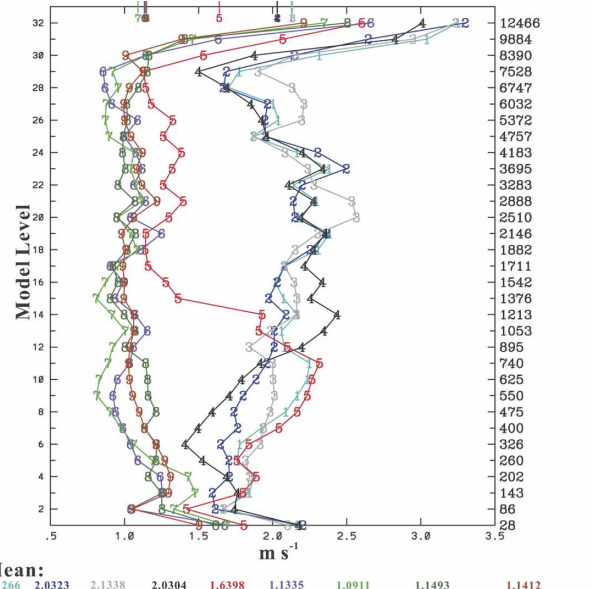


FIG. 13. Vertical profiles of the 30-h-averaged MAE for MM5-simulated wind speed in CAPTEX-83 episode 1 (1200 UTC 18 Sep–1800 UTC 19 Sep 1983) on the 4-km verification domain. The 32-layer mean statistics are plotted on the top of the chart, with the digital values also included above the experiment key at the bottom of the figure.

in the atmosphere above the PBL and the first two model layers near the surface. In much of the PBL, however, the MAE for experiment MB1FA is even larger than that in the baseline experiment MB1. This is likely because the analyses are too coarse to represent the structure within the PBL and have a detrimental effect because the Analysis FDDA tends to destroy the mesoscale structures that are naturally produced by the MM5 within the PBL at 4-km grid resolution. This result confirms why analysis nudging is not recommended for fine-resolution domains, especially in the PBL or lower troposphere (e.g., Stauffer and Seaman 1994; Shafran et al. 2000).

Further inspection of the results in Fig. 13 indicates that experiment MB2MRF, using the MRF PBL scheme, is one of the worst experiments in the PBL. Experiment MB2 (using enhanced vertical mixing in GS PBL scheme) shows a distinct improvement over the baseline experiment MB1, and further improvement is evident when using experiment MB2KF (KF on the 4-km-resolution domain).

Figure 14 shows the 30-h-averaged ME of wind speed for all experiments. It is shown that experiment MB2MRF using the MRF PBL produces the worst results. Simulated wind speeds show negative biases as large as  $1.5 \text{ m s}^{-1}$  for experiment MB2MRF at 1.2 km AGL. Figure 14 also indicates that wind speed tends to

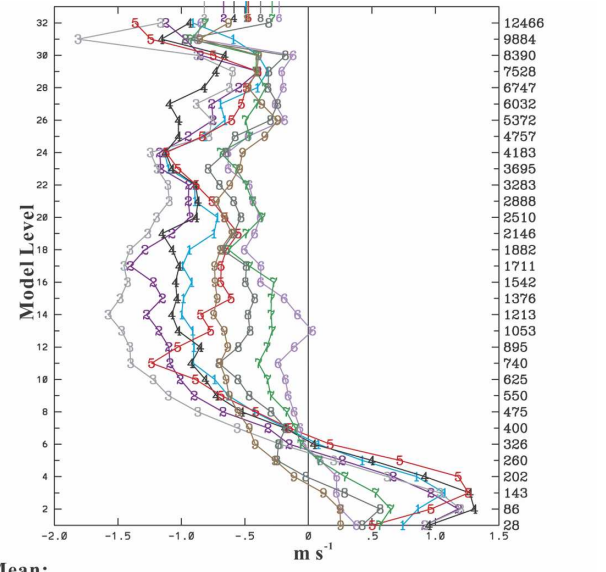


FIG. 14. As in Fig. 13, but for ME of wind speed.

be too fast in the lowest 300 m AGL and too slow above, with use of Obs FDDA tending to produce the best simulations for wind speed in experiments MB1FO, MB2KFFO, and MB2GRFO.

Inspection of the 30-h-averaged values of MAE wind direction in Fig. 15 indicates that experiments MB1 and MB2MRF have the largest model error and experiment MB2KFFO has the smallest error. It is shown that using Obs FDDA tends to produce the smallest model error

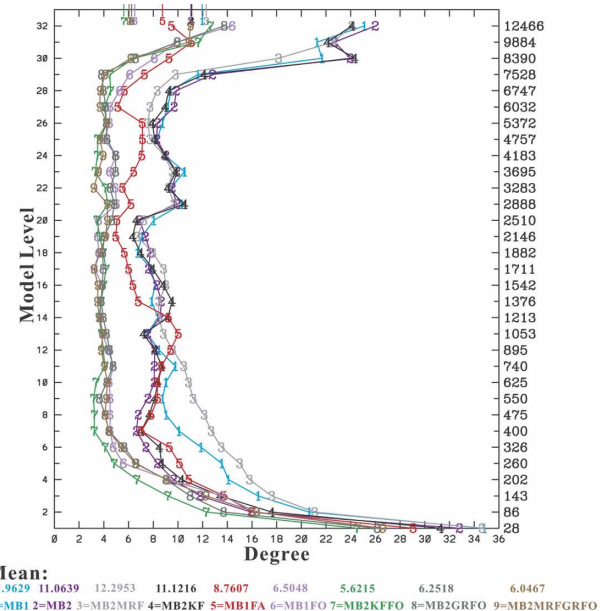


FIG. 15. As in Fig. 13, but for MAE of wind direction.

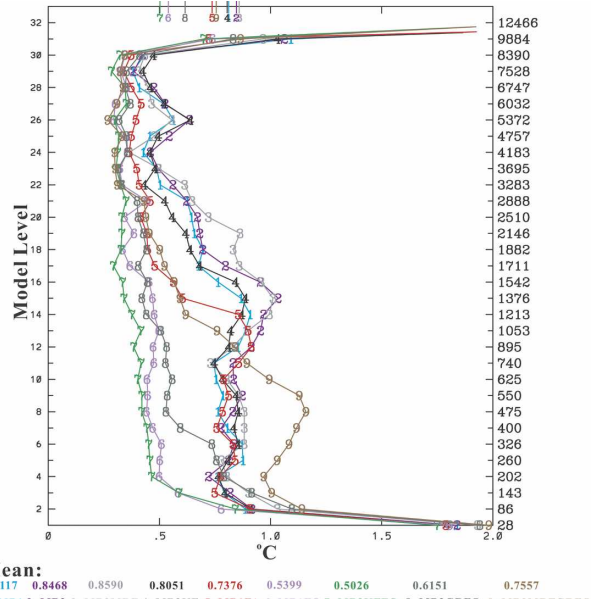


FIG. 16. As in Fig. 13, but for MAE of temperature.

in simulated wind direction, with Obs FDDA combined with use of a CPS being somewhat more effective than the Obs FDDA alone. On average, experiment MB2KFFO is the best Obs FDDA experiment. Using Analysis FDDA shows much greater improvement above the PBL, with much reduced positive effects within the PBL. However, use of the MRF PBL produces the worst result for wind direction in the PBL (lowest 1 km AGL) and also for the average value over all layers. The baseline experiment MB1 also has a relatively large wind direction error in the PBL, and enhancing the vertical mixing in the GS PBL in experiment MB2 produces marked improvements in the PBL.

In summary, when combining wind speed and wind direction errors as vector wind difference (VWD) error, the Obs FDDA experiments produce the lowest VWD errors for both the vertical profiles and at the surface. Experiments MB2KFFO, MB2GRFO, and MB2MRFGRFO errors are all within  $0.1\text{--}0.2\text{ m s}^{-1}$ , with MB2MRFGRFO results being slightly better than the other two at the surface and experiment MB2KFFO (Obs FDDA and KF) producing the best overall wind results. The experiment MB2MRF results are generally worse than all of the other experiments (not shown).

## 2) TEMPERATURE FIELD

Figure 16 shows the vertical profiles of the 30-h-averaged MAE of temperature. It is evident again that the Obs FDDA plays the most significant role in reducing the model error in temperature, with experi-

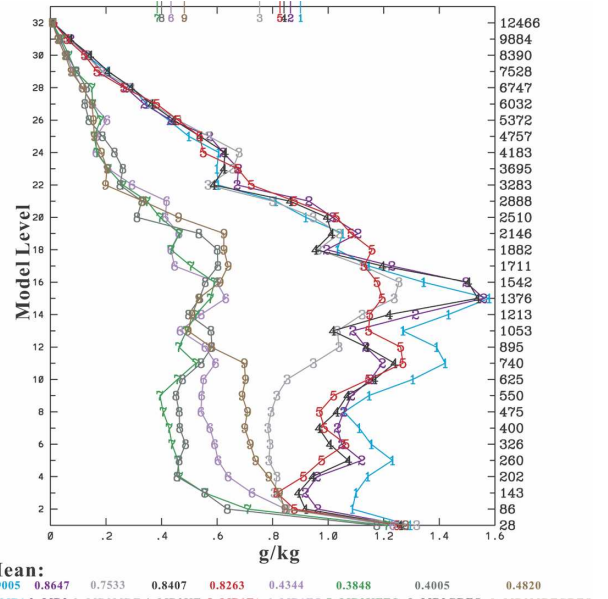


FIG. 17. As in Fig. 13, but for MAE of water vapor mixing ratio.

ment MB2KFFO (which uses both Obs FDDA and KF) having the smallest MAE error. It is encouraging that use of KF along with Obs FDDA (experiment MB2KFFO) is producing smaller errors than using Obs FDDA alone (experiment MB1FO). Experiment MB2GRFO is not as good as MB2KFFO and MB1FO. However, experiment MB2MRFGRFO, which uses MRF PBL, Grell CPS, and Obs FDDA, shows significant degradation in temperature, especially in the PBL (worst experiment in the lowest 1 km AGL). Experiment MB1FA that uses Analysis FDDA shows most of its reduction of MAE in the layers above 1 km AGL. However, below 1 km AGL, where the thermal and moisture nudging are completely turned off, the MB1FA results are very good when compared with the other experiments (MB2, MB2MRF, and MB2KF). The potential degradation of these fields by assimilating coarse temporal and/or spatial resolution mass data is thus minimized by not assimilating these thermal or moisture fields in the lowest 1 km.

## 3) WATER VAPOR MIXING RATIO

Figure 17 shows the vertical profiles of the 30-h-averaged MAE of model-simulated water vapor mixing ratio for all experiments. It is shown that Obs FDDA again produces the best model results for the moisture field, with experiment MB2KFFO (combination of Obs FDDA and KF) being better than experiment MB2GRFO (combination of Obs FDDA, GS PBL, and

Grell CPS). Experiment MB1FO (using Obs FDDA alone) is better than experiment MB2MRFGRFO. When the MRF scheme is used in experiment MB2MRFGRFO, the MM5 again produces some degradation in comparison with the other Obs FDDA experiments in the PBL. Comparisons among all other experiments in the PBL indicate that the baseline experiment MB1 has the largest MAE error for simulated mixing ratio. Although the experiments including experiment MB1FA, MB2, MB2MP, and MB2KF show some positive effects in reducing MAE error, experiment MB2MRF indicates an even larger reduction in MAE. As discussed earlier, the MRF PBL scheme tends to dry the boundary layer possibly because of stronger mixing that causes deeper boundary layers (even at night as in Fig. 4). Notice that experiment MB1FA in which analysis nudging of moisture is not used in the PBL is among the best non-FDDA experiments for reasons discussed earlier for the temperature field.

*c. Does increasing the horizontal resolution always produce better simulations?*

To compare the best MM5-simulated fields between the 12- and 4-km grid resolutions, a new experiment MB2KFFO\_12KM is conducted. This experiment is based on the model configuration of experiment MB2KFFO, but applied to the 12-km-resolution domain. Instead of using Analysis FDDA on the 12-km domain as in experiment 2D\_12KM from Deng et al. 2004, Obs FDDA is applied to the 12-km domain in experiment MB2KFFO\_12KM. Thus, the physics packages (KF, GS PBL) and FDDA techniques (Obs FDDA) used in MB2KFFO\_12KM are identical to those used in experiment MB2KFFO.

Figure 18 shows the vertical profiles of the 30-h-averaged MAE of model-simulated wind speed, direction, temperature, and water vapor mixing ratio for experiments MB2KFFO and MB2KFFO\_12KM. Experiment 2D\_12KM is added to all of the figures as a benchmark representing the best results from the previous study (Deng et al. 2004). It is shown that the profile-averaged wind speed MAE from the best 4-km experiment presented above (experiment MB2KFFO) is larger than that on the 12-km-resolution domain and verified over the 4-km-resolution domain. The 12-km results from Deng et al. (2004) using Analysis FDDA (experiment 2D\_12KM) have an average error about 50% larger than that of the other two experiments. However, the MAE of the simulated wind direction (Fig. 18b) is smaller on the 4-km domain than that on the 12-km domain, with the largest differences (e.g.,

4°–5°) found in the PBL. Again, the 12-km results from the previous study produced error levels about 50% higher than those in this study. For the temperature field, Fig. 18c shows that the 4- and 12-km Obs FDDA solutions are very similar. The temperature errors from the previous study are about 2 times those of the current study. Last, Fig. 18d shows that the model-simulated moisture field is better on the 12-km-resolution domain than that on the 4-km-resolution domain. Therefore, the larger 4-km horizontal resolution does not necessarily produce better model simulations, when using the best model configuration, at least for this convectively unstable case, but the use of Obs FDDA and a CPS on the 4-km domain make the 4- and 12-km results more comparable, and these results are much better than the 12-km Analysis FDDA results previously reported for this case.

## 6. Conclusions

To improve the MM5 simulations on the 4-km grid where the previous study by Deng et al. (2004) indicated that simulation of the 18–19 September 1983 CAPTEX case had detrimental effects on the meteorological solutions, a series of experiments was designed to address model sensitivities on the 4-km-resolution domain to use of Analysis FDDA versus Obs FDDA, planetary boundary layer (PBL) turbulence, mixed-phase microphysics, CPS, and enhanced horizontal diffusion.

The baseline experiment (experiment MB1) used version 3.6 of the MM5 modeling system without FDDA. It reproduced the spurious convective system reported in the original study. Statistical analysis showed that experiment MB1 had relatively large MAE in the model-simulated fields. Use of FDDA on the 4-km-resolution domain reduced both precipitation amount and areal coverage relative to the baseline experiment, but FDDA alone could not completely eliminate the spurious convective system. Statistical results indicated that use of FDDA made a significant contribution toward reducing the model errors. It was shown that using Analysis FDDA of surface wind in the boundary layer based on conventional data had some detrimental effects in the PBL. The use of Obs FDDA produced much better results, as expected, on these finer scales.

Enhanced vertical mixing in the GS PBL scheme showed marked improvements in the simulated wind and mass fields in comparison with the baseline. However, it was apparent that using the enhanced vertical mixing alone did not alleviate the problem with excessive gridpoint convection on the 4-km-resolution domain.

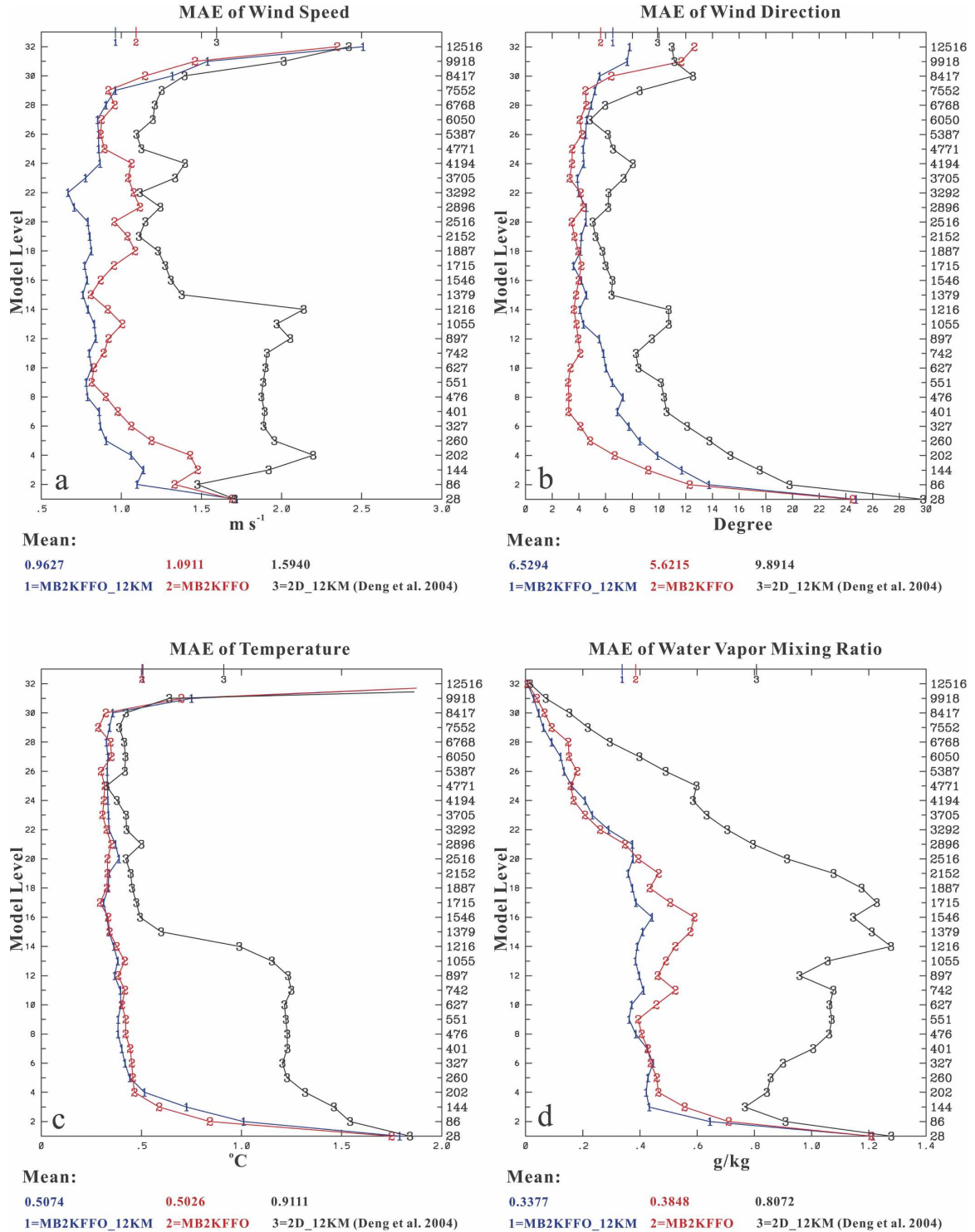


FIG. 18. Vertical profiles of the 30-h-averaged MAE for MM5-simulated fields in CAPTEX-83 episode 1 (1200 UTC 18 Sep–1800 UTC 19 Sep 1983) on the 4-km verification domain for expts MB2KFFO\_12KM (curve 1), MB2KFFO (curve 2), and 2D\_12KM in (Deng et al. 2004) (curve 3): (a) wind speed, (b) wind direction, (c) temperature, and (d) water vapor mixing ratio. The 32-layer mean statistics are plotted on the top of the chart, with the digital values also included above the experiment key at the bottom of each panel.

When the MRF PBL scheme was applied in lieu of the GS PBL scheme in experiment MB2MRF, MM5 produced a significantly worse simulation in the model-simulated precipitation field because the spurious convection had spread to a much larger area, associated with an even larger area of disturbed flow with outflow boundaries and cold pools. Statistical evaluation indicated that experiment MB2MRF produced degraded model simulations in all fields including wind speed, wind direction, and temperature. The only improvement (mainly during nighttime) was in the water vapor mixing ratio field and was likely caused by the overestimation of the PBL depth.

Use of mixed-phase microphysics (experiment MB2MP) produced a precipitation pattern that showed enhanced and more localized precipitation and sometimes stronger gridpoint storms. Experiments using enhanced horizontal diffusion (e.g., experiment MB2DIF1) suggested that use of larger horizontal diffusion alone as a solution to this gridpoint storm problem was largely ineffective and could also smooth out realistic mesoscale wind structure produced by the model.

When a CPS was applied to the 4-km grid (experiment MB2KF), the model-simulated nonconvective rain produced by the explicit microphysics was significantly reduced. The convective scheme produced light or no precipitation in northwest Pennsylvania (at 30 h) where gridpoint-type storms had developed in all of the other experiments. Statistical score comparisons with the baseline experiment MB2 indicated that use of KF on the 4-km-resolution domain had produced some improvements for the model-simulated fields of wind speed, wind direction, temperature, and mixing ratio.

Combining Obs FDDA with KF or Grell CPS in experiments MB2KFFO, MB2GRFO, and MB2MRFGRFO produced the best overall results in both the subjective and statistical evaluations, with Obs FDDA and KF being somewhat better than Grell. These experiments did not produce the spurious mesoscale convective system at 30 h, which allowed the simulated low-level flow at this time to be more consistent with the observations. Thus, use of the combination of Obs FDDA and a CPS on the 4-km-resolution domain seemed to have the most significant positive impact on the model solutions in this CAPTEX-83 case, with the best overall results obtained using Obs FDDA and KF. Note that in MB2MRFGRFO the MRF PBL problem may be reduced because of the use of FDDA and CPS. The unrealistic PBL depth does not do as much damage because the wind and moisture field (moisture convergence) are also affected by FDDA and CPS, and not only by the turbulent vertical mixing.

Finer resolution does not always produce better simulations, especially for convectively unstable environments. Use of a CPS and Obs FDDA on the 4-km-resolution domain produced results more comparable to those using CPS and Obs FDDA on a 12-km-resolution domain, and this represented a further improvement to the best MM5 simulation using Analysis FDDA on the 12-km domain reported in Deng et al. (2004).

Note that although this is only one case study, this case is representative of midlatitude frontal rain and deep convection cases, so these results should be generally representative of other cases. Additional cases are still needed to determine the added value of this approach. It must also be pointed out that use of a CPS such as the Kain Fritsch scheme at 4-km grid resolution for deep convection violates the underlying assumption that the size of the subgrid deep convective elements being parameterized are much smaller than the grid size. It is also clear that, in general, explicit microphysics alone cannot completely represent deep convection on these 4-km grid scales and some type of parameterization is needed. Because there is no readily available approach to do this parameterization, it presents a serious dilemma when using 4-km grids to simulate deep convective environments. The current results show that use of a CPS on the 4-km grid may still be helpful in these situations in which 4-km resolution is desired and explicit microphysics alone produces grossly unrealistic QPF. These findings will be further investigated in phase two of this study using the new advanced research Weather Research and Forecast (WRF) model (Wicker and Skamarock 2002; Klemp et al. 2003).

The WRF model is a new state-of-the-science meteorological model currently under development and specifically designed for the 1–10-km grid length scales. The WRF uses an Arakawa-C horizontal grid staggering with higher-order spatial and temporal finite-differencing schemes. In addition to updated model physics, including PBL physics, microphysics, and CPS, it also contains cloud-scale 3D subgrid turbulence schemes (Smagorinsky or TKE-predicting schemes). The WRF should be attractive for future air-quality work because of its mass conservation, improved numerics, and expanding physics. Comparison of model performance between MM5 and WRF and lessons learned here can be a significant contribution to developing fine-resolution mesoscale models in the future.

**Acknowledgments.** This work was supported by the Coordinating Research Council (CRC) through Contract A-46. We also appreciate the detailed comments on this work from the CRC reviewers. We acknowledge

John S. Kain and George A. Grell for helpful discussions related to this project. Special thanks are given to Glenn Hunter for his assistance with some of the graphics for this paper.

## REFERENCES

- Arakawa, A., and W. H. Schubert, 1974: Interaction of a cumulus cloud ensemble with the large-scale environment, Part I. *J. Atmos. Sci.*, **31**, 674–701.
- Bryan, G. H., J. C. Wyngaard, and J. M. Fritsch, 2003: Resolution requirements for the simulation of deep moist convection. *Mon. Wea. Rev.*, **131**, 2394–2416.
- Deng, A., N. L. Seaman, and J. S. Kain, 2003: A shallow-convection parameterization for mesoscale models. Part I: Submodel description and preliminary applications. *J. Atmos. Sci.*, **60**, 34–56.
- , —, G. K. Hunter, and D. R. Stauffer, 2004: Evaluation of interregional transport using the MM5-SCIPUFF system. *J. Appl. Meteor.*, **43**, 1864–1886.
- Dudhia, J., 1989: Numerical study of convection observed during the Winter Monsoon Experiment using a mesoscale two-dimensional model. *J. Atmos. Sci.*, **46**, 3077–3107.
- , 1993: A nonhydrostatic version of the Penn State/NCAR mesoscale model: Validation tests and simulation of an Atlantic cyclone and cold front. *Mon. Wea. Rev.*, **121**, 1493–1513.
- Grell, G. A., 1993: Prognostic evaluation of assumptions used by cumulus parameterizations. *Mon. Wea. Rev.*, **121**, 764–787.
- , J. Dudhia, and D. R. Stauffer, 1994: A description of the fifth generation Penn State/NCAR mesoscale model (MM5). NCAR Tech. Note NCAR/TN-398+STR, 138 pp.
- Hong, S.-Y., and H.-L. Pan, 1996: Nonlocal boundary layer vertical diffusion in a medium-range forecast model. *Mon. Wea. Rev.*, **124**, 2322–2339.
- Kain, J. S., 2004: The Kain–Fritsch convective parameterization: An update. *J. Appl. Meteor.*, **43**, 170–181.
- , and J. M. Fritsch, 1990: A one-dimensional entraining/detraining plume model and its application in convective parameterization. *J. Atmos. Sci.*, **47**, 2784–2802.
- , and —, 1993: Convective parameterization for mesoscale models: The Kain–Fritsch scheme. *The Representation of Cumulus Convection in Numerical Models*, Meteor. Monogr., No. 46, Amer. Meteor. Soc., 165–170.
- Klemp, J. B., W. C. Skamarock, and O. Fuhrer, 2003: Numerical consistency of metric terms in terrain-following coordinates. *Mon. Wea. Rev.*, **131**, 1229–1239.
- Mlawer, E. J., S. J. Taubman, P. D. Brown, M. J. Iacono, and S. A. Clough, 1997: Radiative transfer for inhomogeneous atmospheres: RRTM, a validated correlated- $k$  model for the longwave. *J. Geophys. Res.*, **102** (D14), 16 663–16 682.
- Molinari, J., and M. Dudek, 1992: Parameterization of convective precipitation in mesoscale numerical models: A critical review. *Mon. Wea. Rev.*, **120**, 326–344.
- Reisner, J., R. M. Rasmussen, and R. T. Bruintjes, 1998: Explicit forecasting of supercooled liquid water in winter storms using the MM5 mesoscale model. *Quart. J. Roy. Meteor. Soc.*, **124**, 1071–1107.
- Schroeder, A. J., D. R. Stauffer, N. L. Seaman, A. Deng, A. M. Gibbs, G. K. Hunter, and G. S. Young, 2006: An automated high-resolution, rapidly relocatable meteorological nowcasting and prediction system. *Mon. Wea. Rev.*, **134**, 1237–1265.
- Seaman, N. L., 2000: Meteorological modeling for air quality assessments. *Atmos. Environ.*, **34**, 2231–2259.
- Shafran, P. C., N. L. Seaman, and G. A. Gayno, 2000: Evaluation of numerical predictions of boundary layer structure during the Lake Michigan Ozone Study. *J. Appl. Meteor.*, **39**, 412–426.
- Smagorinsky, J., S. Manabe, and J. L. Holloway Jr., 1965: Numerical results from a nine-level general circulation model of the atmosphere. *Mon. Wea. Rev.*, **93**, 727–768.
- Stauffer, D. R., and N. L. Seaman, 1990: Use of four-dimensional data assimilation in a limited-area mesoscale model. Part I: Experiments with synoptic-scale data. *Mon. Wea. Rev.*, **118**, 1250–1277.
- , and —, 1994: On multi-scale four-dimensional data assimilation. *J. Appl. Meteor.*, **33**, 416–434.
- , —, and F. S. Binkowski, 1991: Use of four-dimensional data assimilation in a limited-area mesoscale model. Part II: Effects of data assimilation within the planetary boundary layer. *Mon. Wea. Rev.*, **119**, 734–754.
- , R. C. Munoz, and N. L. Seaman, 1999: In-cloud turbulence and explicit microphysics in the MM5. *Proc. Ninth PSU/NCAR Mesoscale Model Users' Workshop*, Boulder, CO, NCAR, 177–180.
- , A. Deng, A. M. Gibbs, G. K. Hunter, G. S. Young, A. J. Schroeder, and N. L. Seaman, 2004: An automated Humvee-operated meteorological nowcast-prediction system for the U.S. Army. *Workshop on Mesoscale and CFD Modeling for Military Applications*, Jackson, MS, Jackson State University. [Available online at <http://www.ahpcrc.org/conferences/JSU-MODELING/>].
- Sykes, R. I., D. S. Henn, S. F. Parker, and R. S. Gabruk, 1996: SCIPUFF—A generalized hazard dispersion model. *Preprints, Ninth Joint Conference on the Applications of Air Pollution Meteorology*, Atlanta, GA, Amer. Meteor. Soc., 184–188.
- Tan, Z., F. Zhang, R. Rotunno, and C. Snyder, 2004: Mesoscale predictability of moist baroclinic waves: Experiments with parameterized convection. *J. Atmos. Sci.*, **61**, 1794–1804.
- Tanrikulu, S., D. R. Stauffer, N. L. Seaman, and A. J. Ranzieri, 2000: A field-coherence technique for meteorological field-program design for air quality studies. Part II: Evaluation in the San Joaquin Valley. *J. Appl. Meteor.*, **39**, 317–334.
- Tao, W.-K., D. Starr, A. Hou, P. Newman, and Y. Sud, 2003: A cumulus parameterization workshop. *Bull. Amer. Meteor. Soc.*, **84**, 1055–1062.
- Weisman, M. L., W. C. Skamarock, and J. B. Klemp, 1997: The resolution dependence of explicitly modeled convective systems. *Mon. Wea. Rev.*, **125**, 527–548.
- Wicker, L. J., and W. C. Skamarock, 2002: Time-splitting methods for elastic models using forward time schemes. *Mon. Wea. Rev.*, **130**, 2088–2097.
- Willmott, C. J., S. G. Ackleson, R. E. Davis, J. J. Feddema, K. M. Klink, D. R. Legates, J. O'Donnell, and C. M. Rowe, 1985: Statistics for the evaluation and comparison of models. *J. Geophys. Res.*, **90**, 8995–9005.
- Zhong, S., and J. Fast, 2003: An evaluation of the MM5, RAMS, and Meso-Eta models at subkilometer resolution using VTMX field campaign data in the Salt Lake valley. *Mon. Wea. Rev.*, **131**, 1301–1322.